Research Article

Experimental Research and Sensitivity Analysis of Mudstone Similar Materials Based on Orthogonal Design

Caoxuan Wen [ID],[1,2] **Shanpo Jia** [ID],[1,2] **Xiaofei Fu,**[1] **Lingdong Meng** [ID],[1] **and Zhenyun Zhao** [ID][1,2]

[1]*Institute of Unconventional Oil and Gas, Northeast Petroleum University, Daqing 163318, China*
[2]*School of Urban Construction, Yangtze University, Jingzhou 434023, China*

Correspondence should be addressed to Shanpo Jia; jiashanporsm@163.com

Due to the strong hydration sensitivity of mudstone, drilling of deep mudstone is difficult and pricy, which results in the study on its physical and mechanical properties inseparable from similar material tests. On these bases, triaxial compression and Brazilian tensile tests of the original mudstone drilled from the caprock of the D5 aquifer structure are carried out. Then, orthogonal experiments of mudstone similar materials with river sand and barite powder as aggregate and cement and gypsum as the binder are conducted, which include 3 factors that, respectively, are mass ratio of aggregate to binder, mass ratio of cement to gypsum, and barite powder content, and each factor contains 5 levels, totalling 25 groups of 150 samples. By comparing the results of mudstone and artificial samples made of similar materials, it is obvious that artificial samples and mudstone are significantly similar in terms of density, compressive strength, elastic modulus, and compressive strength when the aggregate-binder ratio is about 4, 8, 5, and 4, respectively. Further sensitivity analysis showed that the aggregate-binder ratio played a major role in controlling the properties of artificial samples, while the sensitivity of different parameters to the cement-gypsum ratio and barite content was different. The results indicate that the selected raw materials and their proportion are feasible, which can meet similar requirements and can be a reference for similar material experimental research of target mudstone.

1. Introduction

With the rapid development of urban modernization, the demand for oil and gas is increasing, and the construction of gas storage around the city is imperative. However, it is difficult to find depleted oil and gas reservoirs around the city. As the second largest number of existing gas storage reservoirs, aquifer gas storage plays an important role in the construction of gas storage reservoirs around the city, and its construction, operation, and maintenance are inseparable from the study on the mechanical properties of caprock. Due to the limitation of test conditions, it is difficult to carry out field test [1]. It is common practice to prepare rock samples on-site and then conduct experimental study on physical and mechanical properties in laboratory [2]. However, the high hydration sensitivity of mudstone leads to the high cost of drilling and sampling and high difficulty in taking out complete samples. A similar simulation test, as one of three

main research methods with the other two being theoretical derivation and numerical simulation, is widely used in complex geotechnical engineering, for bearing the advantages of strong operability, low cost, short cycle, and wide range of materials that can be simulated [3–6].

First of all, the proper selection and proportioning of raw materials for similar materials are critical to the test [6–9]. At present, selection of raw materials and their proportioning has been widely studied. Wang and Li, Yang et al., and Xi et al. developed similar materials with different raw materials and proportions, all of which are proved to satisfy the physical or mechanical properties of soft rock [10–12]. Li et al. developed a feasible and effective transparent similar material for soft rock with a combination of silicon powder and oil solution, in order to study the internal deformation and fracture process of soft rock in a more intuitive way [13]. In order to improve the test accuracy of similar materials, the stress-strain characteristics of two different materials were

analyzed through uniaxial compression, and the error sources in the preparation and testing process are proposed [14]. Then, a large number of scholars have carried out many large-scale model tests using various similar materials and applied them to different geotechnical engineering. Cheng et al. analyzed the optimization design of low-strength mechanical test and orthogonal test to simulate the mechanical properties of thick coal seam and extra thick coal seam and obtained the influence degree of each component on uniaxial compressive strength [15]. Zhang et al. developed a similar material called iron crystal sand that is mixed with iron ore powder, barite powder, quartz sand, gypsum powder, and rosin-alcohol solution, applied it to the three-dimensional geomechanical model test study of large bifurcation tunnel, and successfully revealed the deformation performance of surrounding rock of bifurcation tunnel [16]. Dai et al. used the materials composed of barite powder, quartz sand, gypsum, and expansive soil as similar materials of salt rock to carry out the model test of Jintan salt rock gas storage, and the results showed that the similar model test technique can be effectively applied to study the long-term stability of salt rock gas storage [17]. Further, some scholars have concentrated on the multiphase coupling characteristics of similar materials, rather than the single phase of solid. Liu and Liu developed a new fluid-solid coupling similar material based on the orthogonal test and verified it in a coal mine floor water inrush by physical simulation test [18]. Zhao et al. and He et al. proposed a similarity criterion for gas "solid-gas" coupling in coal and rock based on the "solid-liquid" coupling similarity theory and conducted multiscale evaluation through experiments and both solid-gas coupled similar materials that can be used in engineering practice [19, 20].

At present, there are few studies on similar materials of mudstone in caprock. Based on the above analysis, the current study aimed to find similar materials of mudstone as caprock and to explore the effects of the contents of similar materials on their density, compressive strength, elastic modulus, and tensile strength. Firstly, laboratory test of original mudstone has been carried out (Section 2). Then, a similarity theory is introduced and similar material mechanics experiments based on orthogonal design are carried out (Section 3) followed by the analysis of similar material test results and sensitivity analysis of influencing factors (Section 4). Furthermore, the similarities and differences between the original mudstone and similar materials are compared, and the prospects of further research on mudstone similar materials in the future are also discussed (Section 5). The innovation of this study is that a new type of artificial rock made of similar material with adjustable proportion of components is proposed to meet the requirements of similarity with mudstone in different parameters.

2. Experiments of Original Rock

Eight large core samples (diameter 50 mm) and one small core sample (diameter 25 mm) (Figure 1) drilled from Permian aquifer tectonic caprock of the 5–1 well in the D5

zone, of which the axial direction is perpendicular to the horizontal direction of the formation, were used to study the mechanical properties of the original rocks in two test schemes: 5 samples for compression test (including uniaxial and triaxial) and 4 for split test. Basic parameters of them are shown in Tables 1 and 2. Mechanical testing and simulation (MTS) machine was used in the experiment of original rock (Figure 2).

2.1. Analysis of Compression Test Results.

The parameters of elastic modulus (E), Poisson's ratio (μ), and compressive strength (σ) were obtained from mudstone triaxial test under different confining pressures (P_C), as shown in Table 3. The elastic modulus and Poisson's ratio were in the ranges 5.59 GPa~9.13 GPa and 0.10~0.14, and the average values of them are, respectively, 7.18 GPa and 0.11. In terms of elastic mechanics parameters, the relative difference in Poisson's ratio is quiet modest, as in elastic modulus it is rather obvious.

The stress-strain curves of mudstone under different confining pressures are shown in Figure 3. Due to the strong heterogeneity of mudstone samples, there are some differences between the test results and normal rock compression tests especially that the compressive strength does not increase with confining pressure. When the confining pressure is 10 MPa, the strain corresponding to peak strength is 1.01%. With the increase of confining pressure, the strain corresponding to peak strength gradually increases, the confining pressure of 20 MPa is 1.47%, the confining pressure of 30 MPa is 2.48%, and the confining pressure of 40 MPa is 3.16%. The stress-strain curves are basically consistent with those of ordinary mudstone; that is, rock failure shows brittleness under low confining pressure (<30 MPa). When the confining pressure rises to 30 MPa, the stress-strain curve shows strain hardening before the peak and strain softening after the peak. When the confining pressure reaches 40 MPa, mudstone shows obvious plastic flow phenomenon and transition from brittleness to plasticity.

Under low confining pressure, the bulk strain of mudstone shows quite apparent dilatancy after the peak, while under high confining pressure all mudstone tests show a state of volume compression. Although the volume of the rock after failure increases to some extent, it still shows compressibility compared with the initial volume. Failure modes of mudstone samples under compression are shown in Figure 3. Under uniaxial compression, brittle fracture failure occurs in mudstones, while shear failure occurs in mudstones under triaxial compression. For sample No. 5, there is only one micro crack on its surface where no other obvious failure characteristic existed. The expansion deformation of the sample exceeded the allowable value set, resulting in the end of the test, and the sample is considered to fail internally (Figure 4).

2.2. Analysis of Splitting Test Results.

The parameter of tensile strength (τ) was obtained through mudstone splitting test, as shown in Table 4. The tensile strength of the

(a)

(b)

(c)

(d)

FIGURE 1: Origin rocks drilled from D5-1 well: (a) argillaceous siltstone, depth of 2315.7 m~2320.9 m; (b) mudstone, depth of 2327.3 m~2331.7 m; (c) mudstone, depth of 2331.7 m~2339.9 m; (d) mudstone, depth of 2339.9 m~2342.6 m.

TABLE 1: Basic parameters of origin rocks for triaxial compression.

No.	Depth (m)	Size ($D \times H$) (mm)	ρ (g·cm^{-3})	Description
1	2323.3	25.94×50.81	2.50	Complete and jointless
2	2342.1	50.08×67.43	2.37	Complete and jointless
3	2328.3	49.31×64.14	2.38	Complete with slight inclined grain
4	2341.5	50.02×93.89	2.36	Complete with horizontal grain
5	2341.6	50.13×82.61	2.36	Complete with horizontal grain

TABLE 2: Basic parameters of origin rocks for splitting tests.

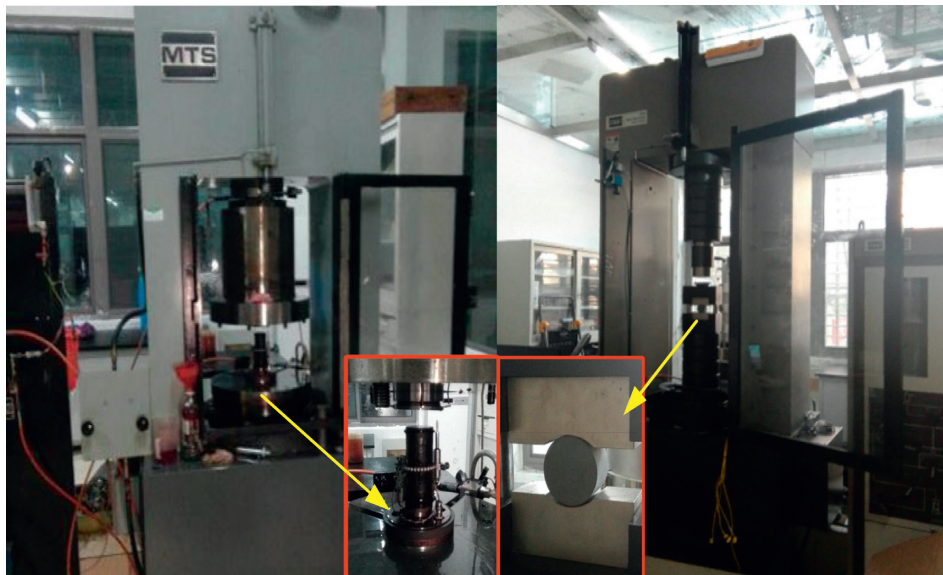| No.	Depth (m)	Size ($D \times H$) (mm)	ρ (g·cm^{-3})	Description
6	2327.9	50.24×44	2.38	Complete with horizontal grain
7	2327.9	49.92×26	2.38	Complete with horizontal grain
8	2317.7	50.07×30	2.45	Complete
9	2317.7	49.60×34.4	2.45	Complete

FIGURE 2: Testing machine used in the experiment of original rock.

TABLE 3: Results of triaxial compression tests.

No.	P_C (MPa)	σ (MPa)	E (MPa)	μ
1	0	64.45	6316.68	0.11
2	10	92.11	9131.15	0.10
3	20	103.20	8651.23	0.14
4	30	93.18	6213.92	0.10
5	40	95.21	5589.32	0.12
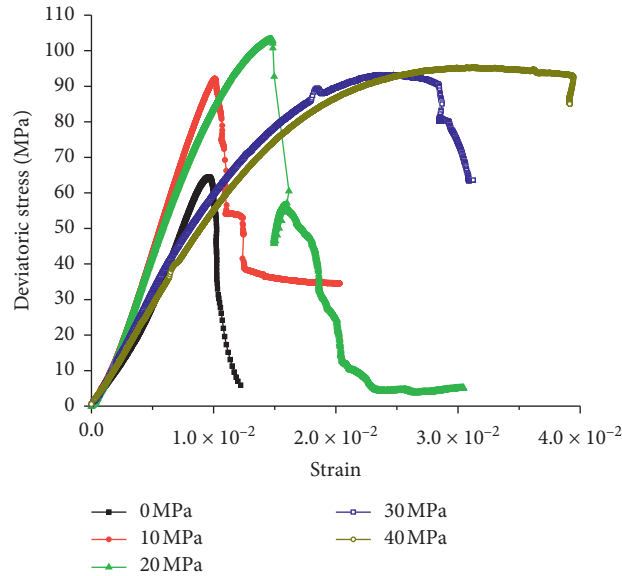
FIGURE 3: Stress-strain curves of triaxial compression samples.

No. 1 $\frac{Before}{After}$ No. 2 $\frac{Before}{After}$ No. 3 $\frac{Before}{After}$ No. 4 $\frac{Before}{After}$ No. 5 $\frac{Before}{After}$
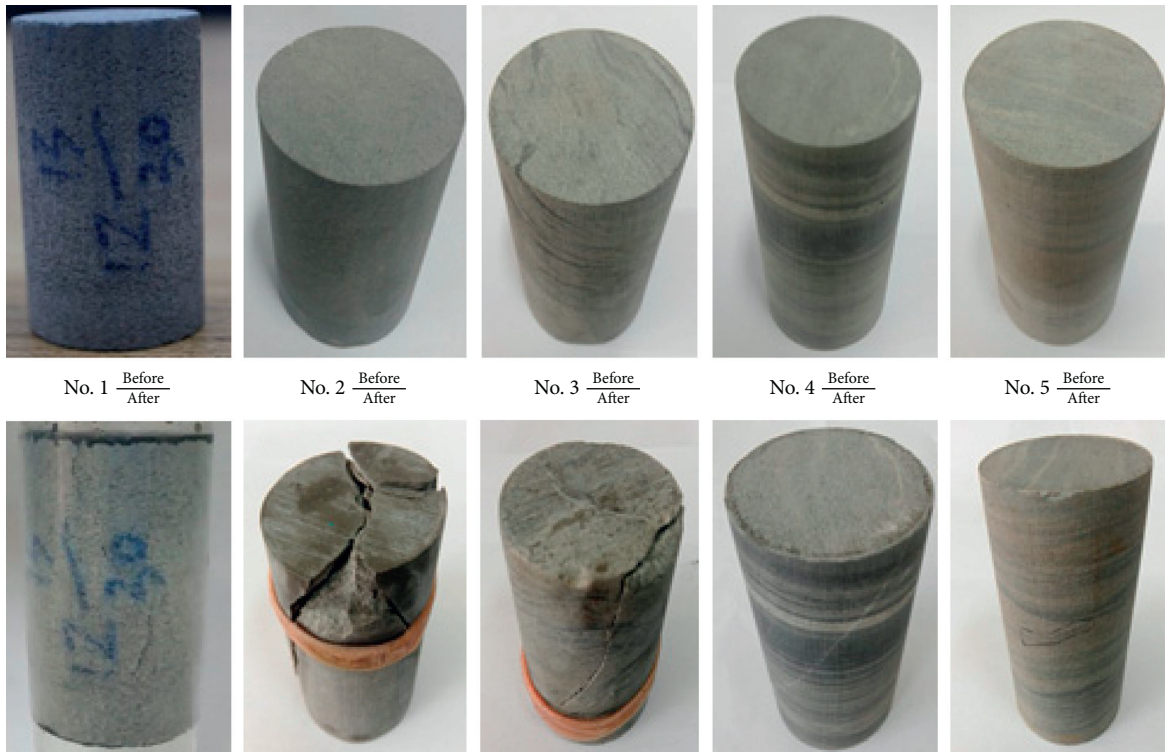
FIGURE 4: Failure modes of triaxial compression samples.

TABLE 4: Results and failure modes of splitting tests.

No.	τ (MPa)	Displacement (mm)	Failure modes
6	7.44	0.433	Splitting occurs along the predetermined loading direction, split into almost symmetrical halves
7	4.15	0.376	Splitting occurs along the predetermined loading direction, split into symmetrical halves
8	4.79	0.326	Splitting occurs along the predetermined loading direction, split into symmetrical halves
9	5.70	0.460	Splitting occurs along the predetermined loading direction, split into symmetrical halves

specimens has a certain discreteness and was in the ranges of 4.15 MPa~7.44 MPa with the average value being 5.52 MPa. The shapes of stress-displacement curves in the splitting tests of mudstones show similarity to some extent, which can be divided into stages of compaction, elastic deformation, and plastic failure, in which the compaction stage is relatively obvious. Once samples for the splitting test reached their maximum load capacity, all of them failed immediately and turned into nearly symmetrical halves (Figure 5).

3. Similar Materials and Methods

3.1. Similarity Theory. Similarity theory, a principle of studying natural similarity phenomena, provides a method to determine the similarity criterion and is the theoretical basis to guide model test. When the prototype and model are similar in geometry, physical and mechanical parameters, and load conditions, the physical and mechanical performance of them would be in similarity. The similarity relation of prototype and model can be derived from the equilibrium, geometric and physical equations, as well as the stress and displacement boundary conditions combined with dimensional analysis method:

$$\left. \begin{array}{l} C_\sigma = C_\gamma C_l = C_E C_\varepsilon \\ C_\sigma = C_E = C_c = C_{\sigma_c} = C_{\sigma_t} \end{array} \right\}, \qquad (1)$$

where $C_\sigma, C_\varepsilon, C_\gamma, C_l, C_{\sigma_c}, C_{\sigma_t}, C_E, C_c$ refer to similarity ratios of stress, strain, severity, geometry, compressive strength, tensile strength, elastic modulus, and cohesion, respectively.

As previously mentioned, the evolution law of compressive strength with confining pressure of mudstone was not consistent with normal rock. Therefore, in order to minimize the influence of formation depth, confining pressure conditions, and other factors and obtain a relatively accurate comparison of mechanical parameters between mudstone and similar materials, only uniaxial compression test and splitting tests were conducted for similar materials.

According to the design of the test scheme, the similarity ratios for geometric similarity, density, and elastic modulus are $C_\gamma = 1.3$, $C_l = 7.5$, and $C_{\sigma_c} = C_{\sigma_t} = C_E = C_\gamma \times C_l = 9.75$. The mechanical parameters of mudstone in the prototype and the model are given in Table 5.

3.2. Selection of Raw Materials and Proportioning Scheme. It is the entity itself, not the model, which can fully reflect all the properties, characteristics, and laws of the entity. The significance of the model is that it can express the main characteristics of the entity, thus exploring more natural laws under limited experimental conditions.

The prerequisite for conducting a model test is to find proper similar materials for the model. The basic requirements of similar materials are: (1) uniformity and isotropic; (2) stable mechanical properties not easily affected by environmental conditions; (3) convenient for manufacture; (4) easy to measure; and (5) short cycle and low cost. In this paper, river sand and barite powder are selected as aggregates, while cement and gypsum are selected as cementing agents. The basic parameters of the raw materials are shown in Table 6.

The proportioning scheme based on orthogonal design includes 3 factors that, respectively, are mass ratio of aggregate to binder (factor A), mass ratio of cement to gypsum (factor B), and content of barite powder (factor C), and each factor contains 5 levels, totalling 25 groups of 150 samples (Tables 7 and 8).

3.3. Test Scheme. According to the standard for test methods of engineering rock mass (in Chinese) [21] and in order to remove the specimen from the mold easily, a mold consisting of one steel bottom plate and eight halve cylinders with a diameter of 50 mm and a height of 100 mm was designed (Figure 6). After the mold was assembled, the samples were prepared according to the steps of weighing, stirring, compacting, demolding, cutting, and numbering (Figure 7).

Microcomputer controlled electrohydraulic servo universal testing machine (WAW-1000b) was used in the compression and splitting tests (Figure 8). Displacement loading was adopted in both tests, and the rate was 0.750 mm/min. The uniaxial compression strength was calculated according to

$$\sigma_c = \frac{P}{A}, \qquad (2)$$

where σ_c is uniaxial compressive strength, P is ultimate load, and A is sample cross-sectional area. And the splitting strength was calculated according to

$$\tau = \frac{2P}{\pi DH}, \qquad (3)$$

where τ is the splitting strength, D is the diameter of the sample, and H is the height of the sample.

4. Deformation and Failure Characteristics and Strength Analysis

4.1. Deformation and Failure Characteristics. The failure process of artificial samples in uniaxial compression can be divided into three stages: compaction stage of cracks, linear
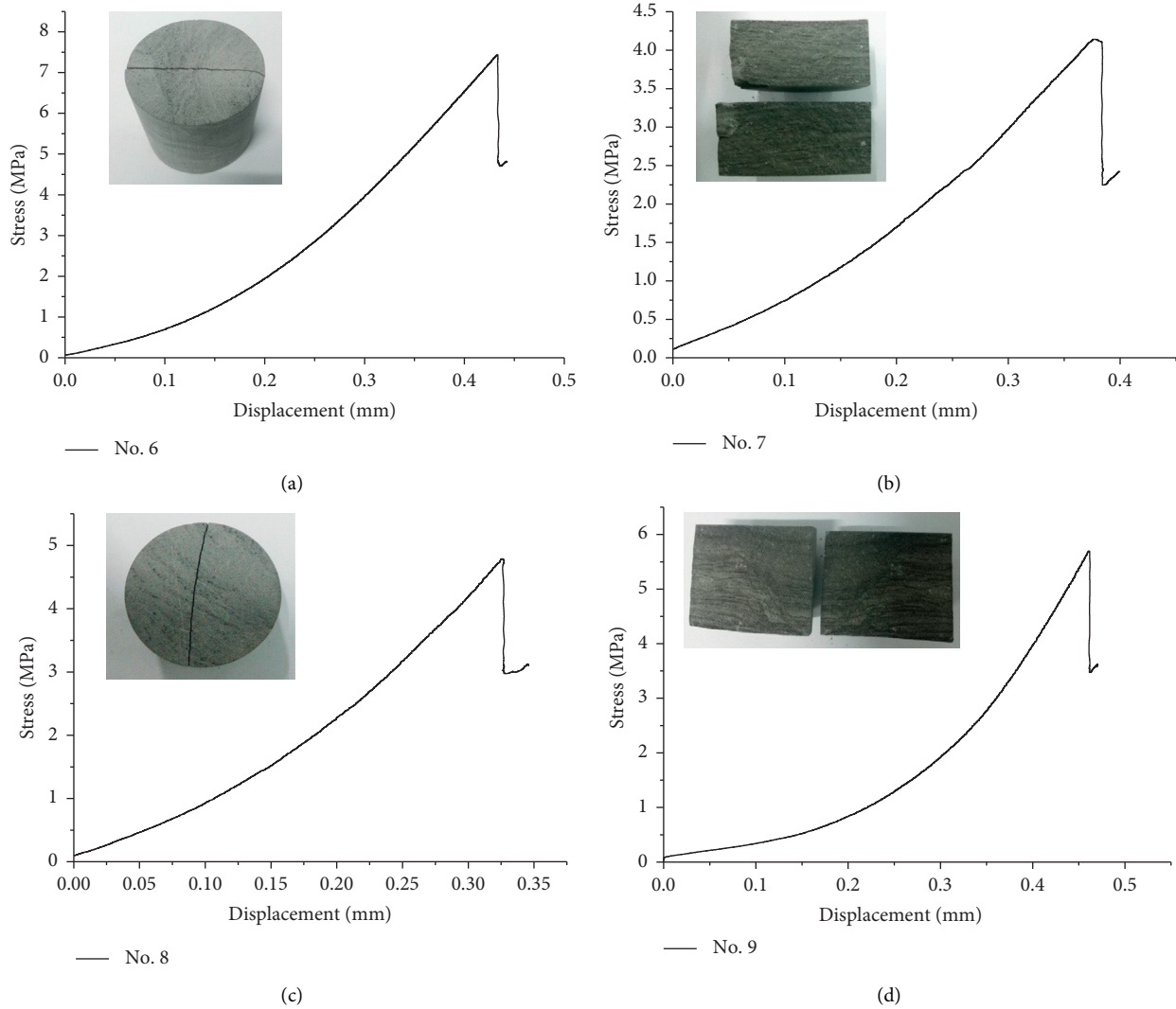
(a)

(b)

(c)

(d)

FIGURE 5: Stress-displacement curves and failure modes of splitting samples: (a) No. 6; (b) No. 7; (c) No. 8; (d) No. 9.

TABLE 5: Target parameters of prototype and model.

	ρ (g/cm^3)	E (MPa)	σ (MPa)	τ (MPa)
Prototype	2.50	6316.68	64.45	5.52
Model	1.92	647.86	6.61	0.57

TABLE 6: Basic parameters of raw materials.

Raw materials		Color	Main ingredient content	Size (mm)	Bulk density (g·cm^{-3})
Aggregate	River sand	Gray-black	$SiO_2 > 90\%$	<1.0	1.65
	Barite content	Gray-white	$BaSO_4 > 90\%$	0.1~0.5	1.48
Binder	Cement	Gray	$CaSiO_3 > 75\%$	0.1~0.5	1.45
	Gypsum	White	$CaSO_4 > 95\%$	0.1~0.5	1.36

elastic stage, and plastic failure stage (Figure 9). In the compaction stage of cracks, the axial load made the cracks in the samples closed under pressure. With the gradual increase of the stress, there is a certain nonlinear deformation in the specimen. The more compressible the pores and cracks in the samples, the greater the continuous deformation in this stage. As the compressible pores and cracks were compressed, the stress-strain curve was basically a straight line inclined upward, which indicates that the samples undergo the linear elastic stage. The linear elastic stages of samples with low aggregate-binder ratio (2 : 1, 4 : 1, and 6 : 1) are more obvious than those of samples with low aggregate-binder

TABLE 7: Orthogonal design of similar materials.

Factors' levels	A	B	C
1	2:1	1:9	0
2	4:1	3:7	10
3	6:1	5:5	20
4	8:1	7:3	30
5	10:1	9:1	40

TABLE 8: Proportioning scheme of similar materials.

No.	A	B	C
1	2:1	1:9	0
2	2:1	3:7	10
3	2:1	5:5	20
4	2:1	7:3	30
5	2:1	9:1	40
6	4:1	1:9	10
7	4:1	3:7	20
8	4:1	5:5	30
9	4:1	7:3	40
10	4:1	9:1	0
11	6:1	1:9	20
12	6:1	3:7	30
13	6:1	5:5	40
14	6:1	7:3	0
15	6:1	9:1	10
16	8:1	1:9	30
17	8:1	3:7	40
18	8:1	5:5	0
19	8:1	7:3	10
20	8:1	9:1	20
21	10:1	1:9	40
22	10:1	3:7	0
23	10:1	5:5	10
24	10:1	7:3	20
25	10:1	9:1	30

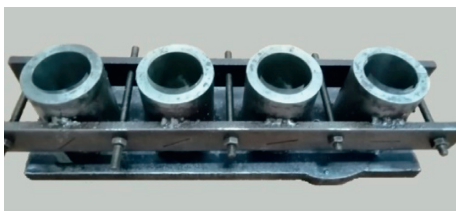Mass of water is 18% of the total mass of raw materials.

FIGURE 6: Preparation of mold.

ratio (8:1 and 10:1). When the elastic ultimate load is reached, samples entered the plastic failure stage. In this stage, the cracks of the samples developed continuously and resulted in irreversible deformation. Then, the slope of the stress-strain curves started to decrease as the stress continued to rise to the ultimate strength. When the stress rose to the ultimate strength, there would be a sudden stress drop accompanied by a clear and loud sound of destruction. After that, all curves showed a softening stage, indicating that similar materials have a certain plastic deformation capacity. In the end, the internal structure of the samples was completely destroyed but remained basically integrated in the surface.

There are three typical failure modes of uniaxial compression: shear failure of single inclined plane (Type A), Y-shaped tensile shear failure (Type B), and pure tensile failure (Type C). The shear failure of single inclined plane is caused by the shear stress on the failure surface exceeding the limit. The main crack is a diagonal crack through the whole sample. The maximum shear stress on the failure surface before the failure is also related to the normal stress on the failure surface; thus this mode of failure can also be called compressive shear failure (Figure 10(a)).

Y-shaped tensile shear failure mode shows the splitting wedge failure mechanism. The friction between the two ends of the samples and the bearing plate of the testing machine prevents the two ends from freely expanding laterally, leading to one of the ends to generate a splitting wedge subjected to three-direction compression. As the wedge displaces downward, the other part of the sample is subjected to tension stress and expands laterally until failure (Figure 10(b)).

Under the action of axial compressive stress, tensile stress will be produced in transverse direction. Pure tensile failure, as a typical failure mode of uniaxial compression, is mainly caused by the transverse tensile stress of exceeding the ultimate tensile strength of the rock, which is the result of Poisson effect (Figure 10(c)).

The shapes of stress-displacement curves in the splitting tests of similar materials can be divided into stages of compaction, elastic deformation, and plastic failure, too (Figure 11). The main failure mechanism is that the tensile stress exceeds the tensile strength of the material itself. Generally, the Brazilian splitting failure mode is that a relatively straight crack runs through the entire disk sample with two loading points as the starting point and ending point (Figure 12(a)). If there are microscopic defects in the sample, the cracks will develop along the direction with more defects. Therefore, some bending sections or associated cracks would exist in some samples (Figure 12(b)).

4.2. Analysis of Factors. From the sample group number 1 to 25, the aggregate content increases and binder content decreases (Table 8). With the increase of the aggregate-binder ratio, the binder is not enough to fill all the pores between aggregates. Although the density of aggregate is greater than that of the binder (Table 6), the difference between the aggregate and cementing agent density is still not enough to compensate for the density reduction caused by the pores. Therefore, the density of samples decreases with the increase of aggregate-binder ratio (Figure 13(a)). For the same reason, the larger the aggregate-binder ratio is, the more internal the pores are in quantity and volume. And the mechanical properties of similar materials largely depend on the cementing performance of binder. Therefore, the compressive strength, tensile strength, and elastic modulus of all the samples decreased with the increase of aggregate-binder ratio (Figures 13(b)–13(d)).
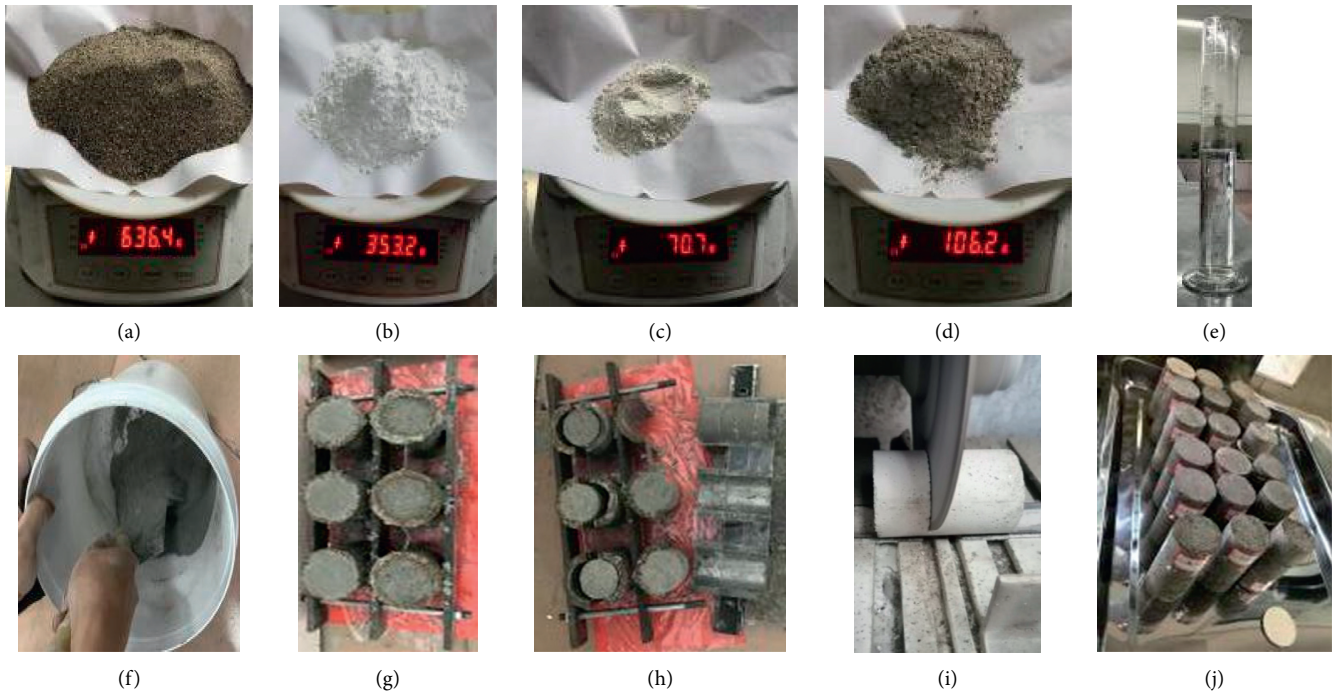
FIGURE 7: Preparation of samples: (a) river sand; (b) barite powder; (c) gypsum; (d) cement; (e) water; (f) stirring; (g) compacting; (h) demolding; (i) cutting; (j) partial samples.
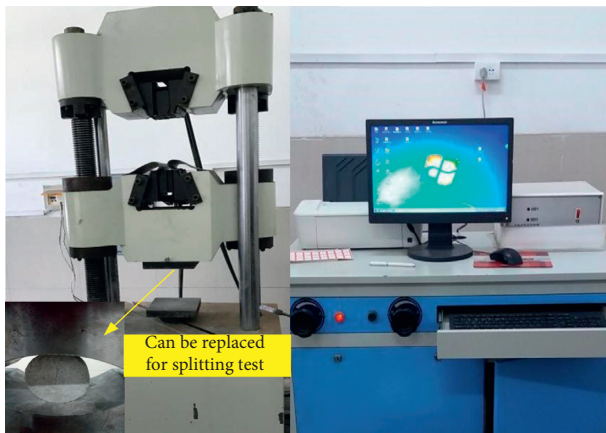

FIGURE 8: Testing machine used in the similar material experiment.

There is a significant negative correlation between the cement-gypsum ratio and uniaxial compressive strength and tensile strength. The smaller the cement-gypsum ratio is, the greater the uniaxial compressive strength and tensile strength are, indicating that, as a cementing agent, the cementing performance of gypsum is obviously better than that of cement (Figures 13(b), and 13(d)). The effect of cement-gypsum ratio on the elastic modulus is not as obvious as that on the strength, yet the elastic modulus tends to decrease with the increase of the cement-gypsum ratio (Figure 13(c)). Since the density of cement and gypsum used in the test is not much different (Table 6), the variation tendency of cement-gypsum ratio on density is not obvious (Figure 13(a)).

As the grain size of barite powder is smaller than that of river sand, better gradation can be formed when the two materials exist simultaneously (Table 6). In the ratio range of this test (0%~40%), the higher the barite content, the smaller the porosity of the sample. Thus, the density of samples increased with the increase of barite powder content (Figure 13(a)). When barite content is 0%, the sample has the most internal defects, and the compressive strength, elastic modulus, and tensile strength are the lowest. When barite powder (10%~40%) was present in the sample formula and gradually increased in content, the elastic modulus of the sample increased steadily, while the compressive strength and tensile strength showed a decreasing trend on the whole, indicating that the increase of barite powder content could significantly improve the brittleness of the sample but had a negative impact on the increase of strength (Figures 13(b)–13(d)).

The horizontal dotted line is the target value of similar material, and the horizontal coordinate values of the point intersecting with the curves are the ratios meeting the similarity requirement. The density, elastic modulus, and tensile strength of the target mudstone are all within the scope of this orthogonal design similar material test (Figures 13(a), 13(c), and 13(d)). As for uniaxial compressive strength, although the cement-gypsum ratio and barite powder content cannot meet the requirements of target mudstone, according to the general trend that uniaxial compressive strength decreases with the increase of cement-gypsum ratio and barite powder content, the cement-gypsum ratio and barite powder content can be increased to meet the requirements.
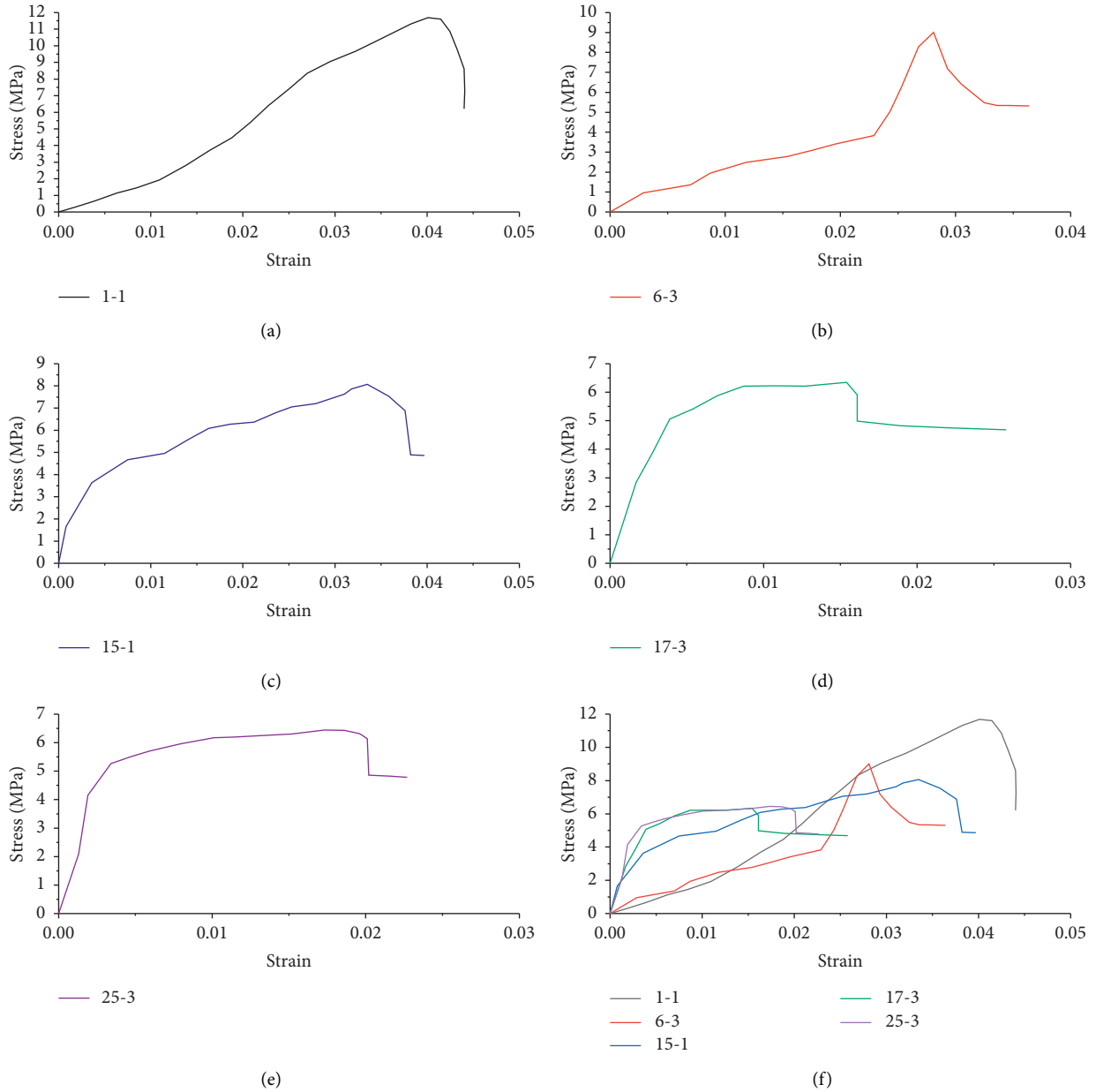
FIGURE 9: Typical stress-strain curves of uniaxial compression tests.

4.3. Sensitivity Analysis. Generally, X_{ij} is defined as the *i*th level value of factor j ($i = 1, 2, ..., n$; j = A, B, C), and Y_{ij} are values obtained from experiments conducted under X_{ij}, and Y_{ij} is a normally distributed random variable. Y_{ijk} are P_1 results obtained by conducting P_1 experiments under X_{ij} ($k = 1, 2, \ldots, P_1$). Then,

$$K_{ij} = \frac{\sum_{k=1}^{P_1} Y_{ijk}}{P_1}, \tag{4}$$

where K_{ij} is the statistical parameter of the j th factor at the i th level.

Normally, $\overline{K_{ij}}$, the average value of K_{ij}, is used to evaluate the results, namely,

$$\overline{K_{ij}} = \frac{\sum_{k=1}^{P_1} Y_{ijk}}{P_1}. \tag{5}$$

Range R_j refers to the difference between the maximum value and the minimum value of the average value of different levels in j factor, which reflects the dispersion degree of a set of data. The expression is as follows:

$$R_j = \max\{\overline{K_{ij}}\} - \min\{\overline{K_{ij}}\}. \tag{6}$$

Range can be used as a parameter to evaluate the significance of a factor, and its value indicates the degree of influence of the factor on the samples. The larger the range is, the greater the influence of this factor on the samples is. The

(a)

(b)

(c)

FIGURE 10: Three types of typical failure modes of uniaxial compression tests: (a) shear failure of single inclined plane; (b) Y-shaped tensile shear failure; (c) pure tensile failure.

factor with the largest range is also the most important factor [22, 23]. Sensitivity analysis of physical and mechanical parameters is shown in Tables 9–12.

5. Discussion

The triaxial test results of the original rocks show that there are some differences between the test results and normal rock under different confining pressures, especially that the compressive strength does not increase with confining pressure. Due to the heterogeneity and different location and depth of the mudstone samples, the discreteness of test results is relatively large. Thus, the results of tests using

Coulomb criterion fitting the cohesion and internal friction angle of rock may have deviated from the reality, and further triaxial compression tests of similar material models may not yield accurate results by taking these as the target parameters. Therefore, uniaxial compression and splitting tests were designed to obtain the physical and mechanical parameters of similar materials and to compare them with the original rocks.

The significance of a model is that it reflects the main properties of an entity rather than all the properties. For example, density reflects the relative mass of sample per unit volume, while elastic modulus reflects the ability of rock to maintain crack opening and expansion. Due to the depth of
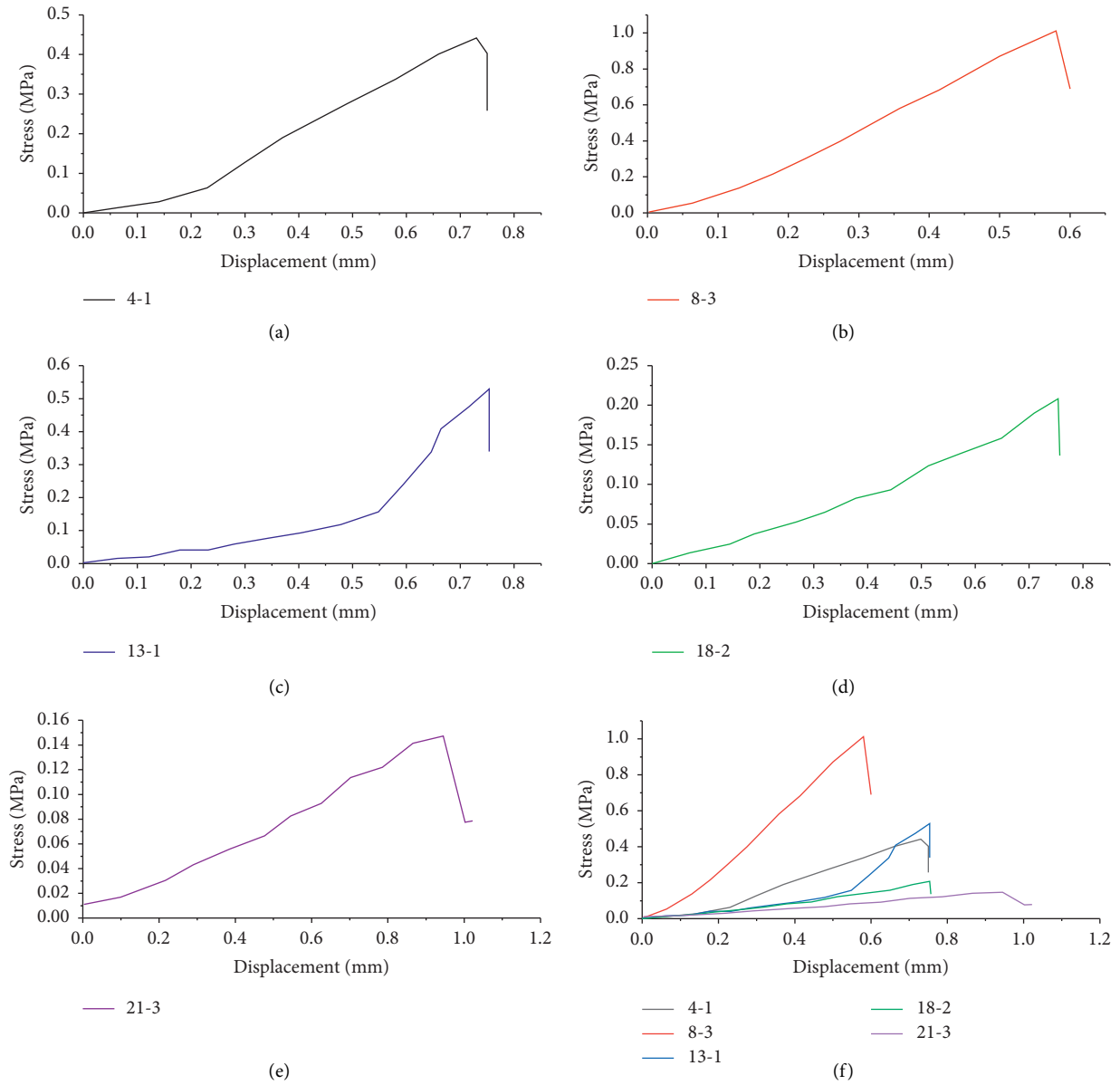
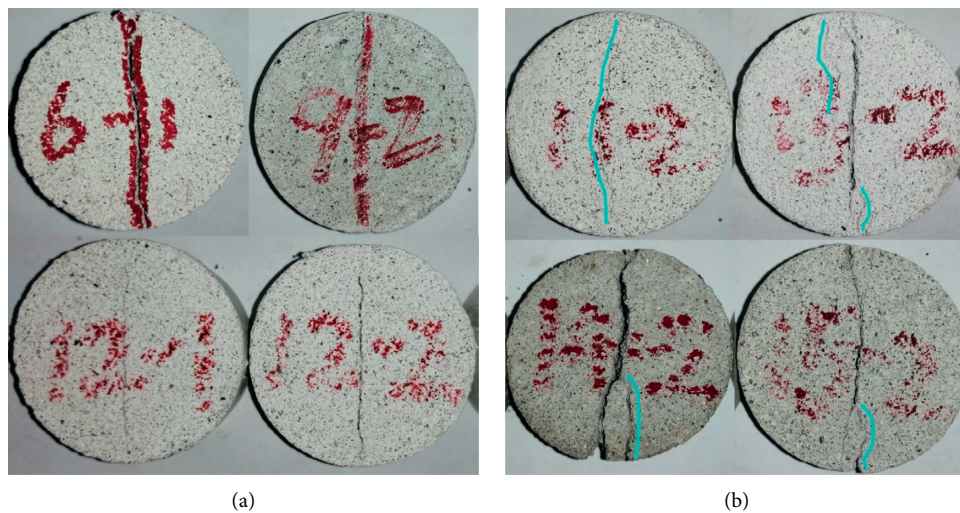Figure 11: Typical stress-displacement curves of splitting tests.

Figure 12: Splitting failure modes: (a) typical splitting failure mode; (b) untypical splitting failure mode.
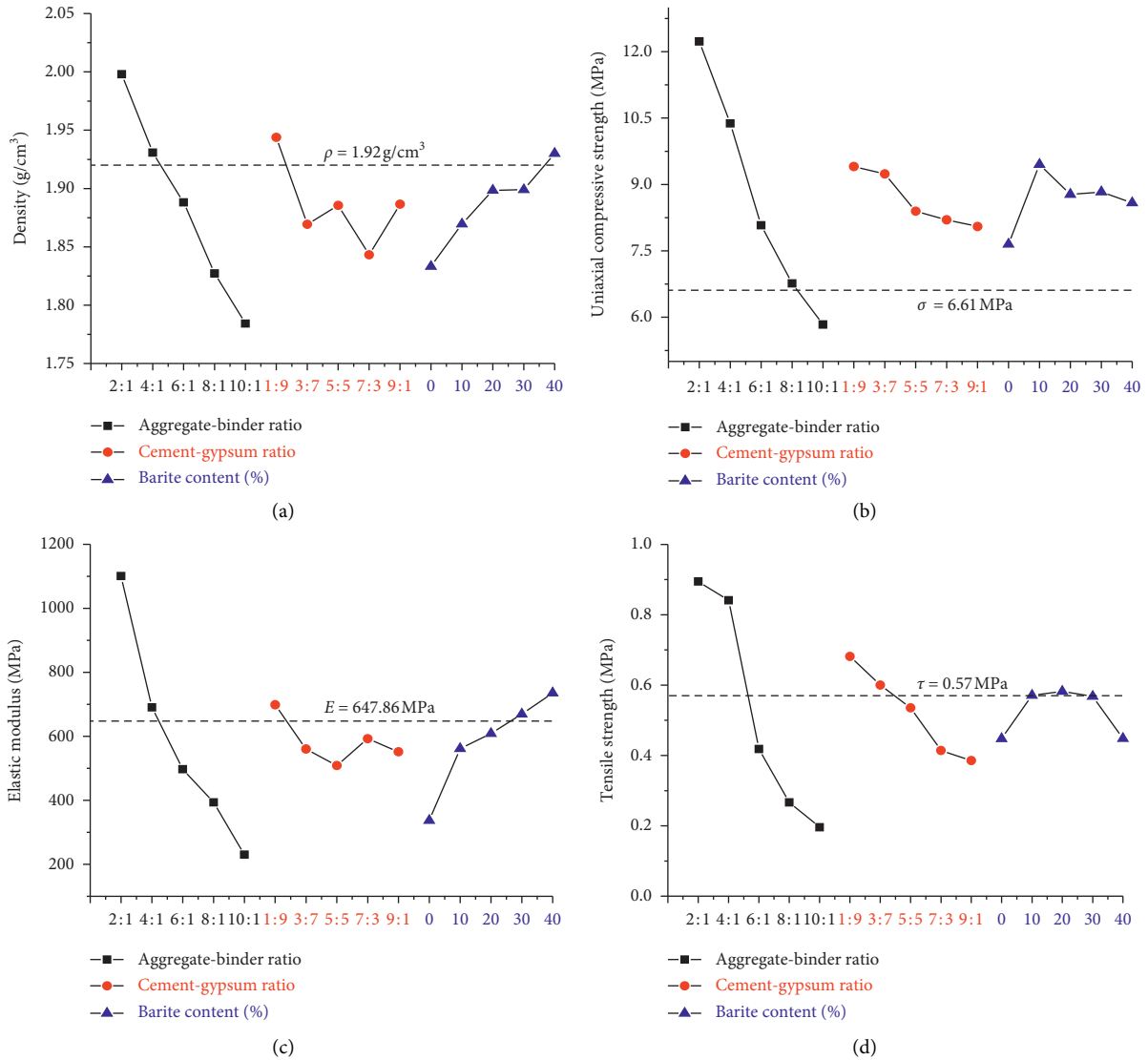
FIGURE 13: Evolution laws of different parameters: (a) evolution laws of density; (b) evolution laws of uniaxial compressive strength; (c) evolution laws of elastic modulus; (d) evolution laws of tensile strength.

TABLE 9: Sensitivity analysis of density to three factors.

Levels of factors	1	2	3	4	5	Range
A	2.00	1.93	1.89	1.83	1.78	0.22
B	1.94	1.87	1.89	1.84	1.89	0.10
C	1.83	1.87	1.90	1.90	1.93	0.10
Sensitivity	$R_A > R_B = R_C$					

TABLE 10: Sensitivity analysis of uniaxial compressive strength to three factors.

Levels of factors	1	2	3	4	5	Range
A	12.23	10.38	8.08	6.76	5.84	6.39
B	9.41	9.24	8.40	8.20	8.05	1.36
C	7.65	9.45	8.78	8.83	8.58	1.80
Sensitivity	$R_A > R_C > R_B$					

gas storage, there is a large vertical downward geostatic stress of the overlying soil layer. The pressure inside the gas storage cavity changes with the gas injection and recovery process. The essence of compressive failure of caprock is that the compressive stress is greater than the compressive strength when the internal pressure is extremely low. When the pressure in the cavity is exceedingly high, tensile stress will occur in the surrounding rock, which may produce tensile failure. The essence of tensile failure is that the tensile

strength of the cover rock is less than the tensile stress. Therefore, it is enough that similar materials can accurately reflect one or several properties of the target entity rather than all properties.

In general, the compressive and tensile stress-strain (displacement) curves of similar material samples are consistent with the curves of the original rock samples and can be divided into three stages, namely, compaction stage,

TABLE 11: Sensitivity analysis of tensile strength to three factors.

Levels of factors	1	2	3	4	5	Range
A	0.89	0.84	0.42	0.27	0.20	0.69
B	0.68	0.60	0.54	0.41	0.39	0.39
C	0.45	0.57	0.58	0.57	0.45	0.13
Sensitivity	$R_A > R_B > R_C$					

TABLE 12: Sensitivity analysis of elastic modulus to three factors.

Levels of factors	1	2	3	4	5	Range
A	1100.92	690.41	497.13	393.67	230.05	870.87
B	698.51	560.37	508.82	592.71	551.77	189.69
C	337.22	561.57	608.50	669.58	735.31	398.09
Sensitivity	$R_A > R_C > R_B$					

linear elastic stage, and plastic failure stage. The average values of density, uniaxial compressive strength, elastic modulus, and tensile strength of different groups of samples ranged from $1.66\,g/cm^3$ to $2.13\,g/cm^3$, $5.25\,MPa$ to $12.49\,MPa$, $84.52\,MPa$ to $1296.34\,MPa$, and $0.16\,MPa$ to $1.20\,MPa$. The level setting of the test factors is reasonable, which includes all the parameters' values that the model should have and provides a suitable adjustment range (Table 5). The ranges of the aggregate-binder ratio to the four target parameters were the largest among all the factors, indicating that the aggregate-binder ratio plays a major role in the adjustment of the four target parameters (Tables 9–12). For density, $R_B = R_C = 0.1\,g/cm^3$, indicating that the cement-gypsum ratio and the barite content have the same sensitivity; thus both of them play a subordinate role relative to the aggregate-binder ratio (Table 9). For uniaxial compressive strength and elastic modulus, $R_B > R_C$, indicating that the uniaxial compressive strength and elastic modulus are more sensitive to barite content; thus the control effect of barite content is more obvious than cement-gypsum ratio (Tables 10 and 12). For tensile strength, $R_C > R_B$, indicating that the tensile strength is more sensitive to barite content; thus the control effect of cement-gypsum ratio is more obvious than barite content (Table 11). In summary, the aggregate-binder ratio plays a major role in controlling the parameters, while cement-gypsum ratio and the barite content play minor roles. Therefore, when adjusting the values of the target parameters, it is necessary to consider the degree of influence of various factors.

Shirmohammadi and Hadadi [24, 25] used fuzzy logic to analyze the data in different situations and obtained reliable conclusions. But, in this study, the sensitivity analysis with range as the indicator is more intuitive. And considering the complexity of parameters and the discreteness of the original rock samples the experiment of similar material merely carries out a comparative analysis on partial, physical, and mechanical parameters. In the future, more original rock tests can be conducted to increase the parameters investigated in the test, such as porosity, permeability, and triaxial compressive strength under different confining pressures, so as to adjust the particle size and formula of aggregate and

cementing agent for obtaining similar material models with more similar properties to the original rock.

6. Conclusions

This study is devoted to finding artificial samples made of similar materials with similar physical and mechanical characteristics of mudstone. The following conclusions are based on laboratory, physical, and mechanical parameter tests of mudstone as caprock with an average depth above 2300 m and artificial samples based on orthogonal design.

(1) The mudstone of the Permian aquifer with an average depth of 2300 m or more was taken as the research target, and the density test, triaxial compression (including uniaxial compression), and Brazilian splitting test were carried out. The obtained values of density, compressive strength, elastic modulus, and Poisson's ratio are, respectively, $2.36\,g/cm^3 \sim 2.50\,g/cm^3$, $64.45\,MPa \sim 103.20\,MPa$, $5.59\,GPa \sim 9.13\,GPa$, and $0.10 \sim 0.14$, with the average value of each of them being $2.40\,g/cm^3$, $89.63\,MPa$, $7.18\,GPa$, and 0.11.

(2) 25 groups of material proportioning schemes totalling 150 samples were designed by orthogonal design method with aggregate-binder ratio, cement-gypsum ratio, and barite content as 3 factors, and five levels were set for each factor. Physical and mechanical parameters such as density, compressive strength, tensile strength, and elastic modulus of similar materials with different proportions were obtained by weighing, uniaxial compression, and splitting tests.

(3) The density, compressive strength, elastic modulus, and tensile strength of artificial samples are, respectively, in the range of $1.78 \sim 2.00\,g/cm^3$, $5.84 \sim 12.23\,MPa$, $230.0 \sim 1100.92\,MPa$, and $0.20 \sim 0.89\,MPa$; $1.84 \sim 1.94\,g/cm^3$, $8.05 \sim 9.41\,MPa$, $508.82 \sim 698.51\,MPa$, and $0.39 \sim 0.68\,MPa$; $1.83 \sim 1.93\,g/cm^3$, $7.65 \sim 9.45\,MPa$, $337.22 \sim 735.31\,MPa$, and $0.45 \sim 0.58\,MPa$ under different levels of aggregate-binder ratio, cement-gypsum ratio, and barite content. The distribution ranges of physical and mechanical parameters obtained from different proportions of similar materials are appropriate, which basically meet the requirements of model test for mudstone similar materials. Most of the samples show good elastic-plastic properties, with obvious segmental stress-strain curves, smooth postpeak softening section, and stable residual strength; in the meanwhile, strength, deformation, and failure characteristics of them are also similar to the original rock, which can provide a basis for the selection and simulation of similar material formulas for mudstone model tests with more parameters in the future.

(4) The sensitivity of various factors to physical and mechanical parameters of materials was analyzed by range analysis method. The results show that the

ratio of aggregate to binder played a major role in controlling the density, compressive strength, elastic modulus, and tensile strength of specimens, while the ratio of cement to gypsum and the content of barite played a minor role in different parameters. The visual analysis diagrams of the influence of each factor on the physical and mechanical parameters of similar materials were obtained, and the evolution laws of the influence of each factor on the parameters of similar materials were analyzed, which provide a direction for the adjustment of specific parameters of similar materials.

Data Availability

The data used to support the findings of this study are included within the article.

Conflicts of Interest

The authors declare no conflicts of interest.

Acknowledgments

References

[1] S. P. Jia, H. Zhang, J. P. Lin et al., "Quantitative assessment of the gas-sealing capacity of the permian claystone caprock for the D5 aquifer gas storage in the linan sag," *Hydrogeology & Engineering Geology*, vol. 43, no. 3, pp. 79–86, 2016, in Chinese.

[2] J. D. Jiang, S. H. Chen, J. Xu, and Q. S. Liu, "Mechanical properties and energy characteristics of mudstone under different containing moisture states," *Journal of China Coal Society*, vol. 43, no. 8, pp. 2217–2224, 2018, in Chinese.

[3] D. Z. Gu, *Similar Materials and Similar Models*, China University of Mining and Technology Press, Xuzhou, China, 1995.

[4] Z. K. Li, D. R. Lu, H. Nakayama, J. H. Xi, and J. S. Sun, "Development and application of new technology for 3D geomechanical model test of large underground houses," *Chinese Journal of Rock Mechanics and Engineering*, vol. 22, no. 9, pp. 1430–1436, 2003, in Chinese.

[5] X. M. Cui, X. X. Miu, D. G. Su, and W. M. Ma, "Error analysis in similar material simulation test of the movement of rock strata and surface," *Chinese Journal of Rock Mechanics and Engineering*, vol. 21, no. 12, pp. 1827–1830, 2002, in Chinese.

[6] S. H. Kim, H. J. Burd, and G. W. E. Milligan, "Model testing of closely spaced tunnels in clay," *Géotechnique*, vol. 48, no. 3, pp. 375–388, 1998.

[7] E. Fumagalli, *Statical and Geomechanical Model*, Springer, New York, NY, USA, 1973.

[8] L. G. Hua and J. Song, "Model and entity," *Systems Engineering and Electronics*, vol. 2, no. 8, pp. 1-2, 1980, in Chinese.

[9] J. M. Sarli, F. Hadadi, and R. A. Bagheri, "Stabilizing geotechnical properties of loess soil by mixing recycled polyester fiber and nano-SiO 2," *Geotechnical and Geological Engineering*, vol. 38, pp. 1–13, 2019.

[10] Y. Y. Wang and J. G. Li, "Experimental study of soft rock similar material by using mixture of asphalt and sea sand," *Journal of Experimental Mechanics*, vol. 28, no. 2, pp. 242–246, 2013, in Chinese.

[11] X. Yang, D. L. Su, B. Zhou, Z. Liu, and C. Y. Zhou, "Experiment study on similarity ratio of similar material for model test on red-bed soft rock," *Rock and Soil Mechanics*, vol. 37, no. 8, pp. 2231–2237, 2016, in Chinese.

[12] J. F. Xi, J. Liang, K. Liang, Z. Q. Wang, and Y. L. Duan, "Study on similar material of soft rock roof for underground coal gasification," *Coal Engineering*, vol. 47, no. 5, pp. 101–104, 2015, in Chinese.

[13] Y. H. Li, Z. B. Lin, X. L. Qin, and P. Liu, "Study of development of transparent rock mass for physical similarity experiment and its mechanical properties," *Journal of China University of Mining & Technology*, vol. 44, no. 6, pp. 977–982, 2015, in Chinese.

[14] F. Luo, B. S. Yang, B. B. Hao, L. H. Sun, and M. M. Fu, "Mechanical properties of similar material under uniaxial compression and the strength error sources," *Journal of Mining & Safety Engineering*, vol. 30, no. 1, pp. 93–99, 2013, in Chinese.

[15] W. Cheng, L. Sun, G. Wang, W. Du, and H. Qu, "Experimental research on coal seam similar material proportion and its application," *International Journal of Mining Science and Technology*, vol. 26, no. 5, pp. 913–918, 2016.

[16] Q. Y. Zhang, S. C. Li, X. H. Guo, Y. Li, and H. P. Wang, "Research and development of new typed cementitious geotechnical similar material for iron crystal sand and its application," *Rock and Soil Mechanics*, vol. 29, no. 8, pp. 2126–2130, 2008, in Chinese.

[17] Y. H. Dai, W. Z. Chen, C. H. Yang, X. J. Tan, and X. L. Jiang, "A study of model test of Jintan rock salt gas storage's operation," *Rock and Soil Mechanics*, vol. 30, no. 12, pp. 3574–3580, 2009, in Chinese.

[18] S. Liu and W. Liu, "Experimental development process of a new fluid-solid coupling similar-material based on the orthogonal test," *Processes*, vol. 6, no. 11, p. 211, 2018.

[19] P. Zhao, R. Zhuo, S. Li, and H. Lin, "Experimental research on the properties of "Solid-Gas" coupling physical simulation similar materials and testing by computer of gas in coal rock," *Wireless Personal Communications*, vol. 102, no. 2, pp. 1539–1556, 2018.

[20] S.-q. He, L.-z. Jin, S.-n. Ou, and X.-h. Ming, "Soft coal solid-gas coupling similar material for coal and gas outburst simulation tests," *Journal of Geophysics and Engineering*, vol. 15, no. 5, pp. 2033–2046, 2018.

[21] GB/T 50266-2013, *Standard for Test Methods of Engineering Rock Mass*, China Planning Press, Beijing, China, 2013.

[22] K. T. Fang and C. X. Ma, *Orthogonal and Uniform Experimental Design*, Science Press, Beijing, China, 2001.

[23] X. R. Chen, *Introduction to Mathematical Statistics*, Science Press, Beijing, China, 1981.

[24] H. Shirmohammadi and F. Hadadi, "Application of fuzzy logic for evaluation of resilient modulus performance of stone mastic asphalt," *Journal of Theoretical & Applied Information Technology*, vol. 95, no. 13, 2017.

[25] H. Shirmohammadi and F. Hadadi, "Assessment of drowsy drivers by fuzzy logic approach based on multinomial logistic regression analysis," *International Journal of Computer Science and Network Security*, vol. 17, no. 4, p. 298, 2017.